Environmental Science and Pollution Research (2022) 29:51815–51826
https://doi.org/10.1007/s11356-022-19558-4

RESEARCH ARTICLE

Pyrolysis behaviors of anaerobic digestion residues in a fixed-bed reactor with rapid infrared heating

Erfeng Hu[1] · Moshan Li[1] · Yishui Tian[2] · Xiaojian Yi[3] · Chongyang Dai[1] · Si Shao[2] · Chenhao Li[1] · Yunfei Zhao[1]

Received: 30 September 2021 / Accepted: 28 February 2022 / Published online: 7 March 2022

Abstract

Fast pyrolysis via rapid infrared heating may significantly enhance the heat transfer and suppress the secondary reaction of the volatiles. The effects of various pyrolysis temperatures on pyrolysis behaviors of anaerobic digestion residues (ADR) were studied in this research utilizing a fixed-bed reactor equipped with rapid infrared heating (IH), as well as to compare the pyrolysis products produced by rapid infrared heating (IH) to those produced by conventional electric heating (EH). Thermogravimetric (TG) analysis revealed that pyrolysis of ADR occurred in three decomposition stages. The results of pyrolysis experiments showed that increasing temperature first raised the bio-oil yield for IH and EH, peaking at 500–600 °C, but thereafter decreased the yield. In contrast to the findings achieved with EH, infrared heating (IH) presented a greater overall bio-oil yield but a lower gas yield. The bio-oil produced by IH increased from 8.35 wt.% at 400 °C to 12.56 wt.% at 500 °C before dropping to 11.22 wt.% at 700 °C. Gaseous products produced by IH have a higher heating value than those generated by EH. Nitrogenous compounds, ketones, and phenols make up the majority of the bio-oil. In the IH bio-oil, nitrogen compounds rose with increasing temperature, while those varied slightly in the EH bio-oil. The phenols content in IH bio-oil was much more than that of EH, exhibiting values of 8.63% and 2.95%, respectively. The findings of the FTIR spectra of biochar indicated that as the temperature increased, the chains of aliphatic side professedly reduced and the structure of biochar became considerably ordered for both heating techniques. The Raman spectra of IH biochar showed that the ratio of A_G/A_D rose progressively from 0.17 to 0.20 as pyrolysis temperature rose from 500 to 700 °C.

Keywords Fast pyrolysis · Secondary reaction · Temperature field · Pyrolysis product · Bio-oil · Biochar

Introduction

Anaerobic digestion (AD) is a highly effective technique for the disposal of agricultural residues, organic solid waste, food waste, and sludge (Wang et al. 2021; González-Arias et al. 2020; Xu et al. 2018a) that can process waste while simultaneously generating green fuels. The processed AD slurry and residue are suitable for use as organic manure, fertilizer mixing, and soil improvement (Meng et al. 2018; Möller and Müller 2012; Xu et al. 2021). However, contaminations such as pathogens, humic acids, and organic matters are frequently found in the anaerobic digestion residues (ADR) (Du et al. 2021; KeChrist et al. 2017), which not only complicate ADR utilization but also pose significant risks to the environmental and human health. Additionally, only around 15 ~ 40% of the energy in the feedstock is converted to biogas after the AD process (Opatokun et al. 2015). To enhance the energy efficiency and sustainability, there is pressing need to improve the resource utilization of ADR.

Pyrolysis can convert the ADR into high-value bio-oil, combustible gases, and biochar through the thermal decomposition and cracking reactions. Pyrolysis also achieves the objectives of ADR disposal in a harmless manner and high-efficient cascade usage. Li et al. (2014) examined the energy recovery perspective of ADR formed by anaerobic digestion of manure and straw. They discovered that anaerobic

Responsible Editor: Ta Yeong Wu

✉ Erfeng Hu
ehu@cqu.edu.cn

[1] State Key Laboratory of Coal Mine Disaster Dynamics and Control, Chongqing University, Chongqing 400044, China

[2] Academy of Agricultural Planning and Engineering, Ministry of Agriculture and Rural Affairs, Beijing 100125, China

[3] School of Mechatronical Engineering, Beijing Institute of Technology, Beijing 100081, China

digestion produced 1.5 ~ 2.6 MJ/kg energy, while pyrolysis produced up to 6.1 MJ/kg of energy. The energy recovery efficiency was improved up to 85% by combining digestate with pyrolysis. In a laboratory-scale auger reactor, Liang et al. (2015) investigated the pyrolysis of potato peel and its fermentation residue. The results indicated that the bio-oil and biochar yields via potato peel pyrolysis were 22.7% and 30.5%, respectively, whereas the bio-oil and biochar yields by the pyrolysis of its fermentation residue were 25.6% and 32.2%, respectively. Neumann et al. (2015) pyrolyzed ADR in a continuous pyrolysis reactor operating at a rate of 2 kg/h, suggesting that the heating value of the bio-oil produced at 750 °C was as high as 33.9 MJ/kg, and the oil had a very low moisture content of 1.7 wt.%. It was estimated that more than 91% of the energy contained in the feedstock was converted into usable products. Additionally, the biochar produced by ADR pyrolysis also showed a significant potential for use. Inyang et al. (2010) conducted the pyrolysis experiments of digestate residue and fresh bagasse samples separately and found that the biochar produced from ADR had a larger surface area, higher ion exchange capacity, and better hydrophobicity than the biochar derived from fresh bagasse. Liu et al. (2020) investigated the properties of pyrolysis products from ADR which was generated from food wastes, concluding that the biochar had an excellent porous structure with a lager specific surface areas, which was beneficial for contaminants removal owing to its high adsorption and catalytic reaction site performance. There was limited work performed on the pyrolysis of ADR, with detailed analysis on the pyrolysis distribution and characterization of pyrolysis bio-oil, gases, and char. Besides, previous studies showed that bench scale reactors with electric heating presented a slow pyrolysis rate for processing ADR. When the heat was transferred into the sample particle by diffusion and convection, the heat gradient caused a prolonged pyrolysis time and the serious secondary reactions of volatiles, implying unclear pyrolysis behavior and products characteristics of ADR.

Both heating rate and pyrolysis temperature are critical parameters that affect the volatilization reaction in the ADR pyrolysis process. Fast pyrolysis rapidly breaks the lignocellulosic structure and suppresses the crosslink of radicals, which may effectively decompose feedstocks with minimized secondary reactions, and the process has garnered considerable scientific interest. The conventional analytical fast pyrolysis may be conducting using Py-GCMS (pyrolysis–gas chromatography/mass spectrometry), thermogravimetric analyzer, or Curie-point pyrolyzer, which can only be loaded with a milligram-level mass sample. As a result, liquid and gaseous products could not be collected and further analyzed. In the recent years, fast pyrolysis through infrared heating has attracted research attentions due to its rapid heating rate (> 10 °C/s) and capacity to load materials at gram level. The infrared heating techniques may enable the sample molecules resonation and rapidly heat transfer, thereby substantially improving the heat transfer process between the heat source and the feedstock through heat conduction. It is advantageous for rapid pyrolysis to reduce the residence time of volatiles. Previous studies on pyrolysis of coal (Xu et al. 2019), biomass (Zhu et al. 2019), and oil shale (Siramard et al. 2017) via rapid infrared heating have been reported. Xu et al. (2019) reported that the tar yield climbed from 9.78 to 13.38% as the infrared heating rate was raised from 6 to 677 °C/min, and the highest rate of tar production was 134% of the G-K test oil yield while heating at 667 °C/min and pyrolyzing at 700 °C. The cedar pyrolysis behaviors using infrared heating were conducted, and the result showed that a faster heating rate favored the generation of acids and furans (Zhu et al. 2019). When oil shale pyrolysis was carried out utilizing rapid infrared heating at 0.1 to 0.5 °C/s, the oil yield rose from 9.5 to 11.1% (Siramard et al. 2017). It is worth noting that the ADR pyrolysis behaviors in both fast pyrolysis and slow pyrolysis aspects have not been reported in preceding literature.

The objective of this work is to investigate the pyrolysis behaviors of ADR in a fixed-bed reactor with rapid infrared heating, which was compared to the results from that with electrically heating. The effects of temperature on behaviors of ADR pyrolysis were investigated, and the composition of gaseous products and bio-oil was determined using gas chromatography (GC) and gas chromatography-mass spectrometry (GC–MS). Furthermore, X-ray diffraction (XRD), Fourier transform infrared spectroscopy (FTIR), and Raman spectrum were employed to characterize the biochar. From analyses of tar components and char characteristics, this work suggested the feasibility of the rapid infrared heating pyrolysis in obtaining a higher tar yield than the electrical heating, as well as an in-depth knowledge of the fast pyrolysis behaviors of ADR.

Material and methods

Materials

Anaerobic digestion residues from Da Xing District of Beijing, China, was used in this study. ADR is comprised of agricultural waste, manure from animals and poultry, and sludge. After 12 h of drying at 105 °C, the dried ADR samples was crushed and sieved to a size below 80 mesh. Proximate analysis of ADR (wt.%, on dry basis) was 4.48 wt.% moisture, 41.88 wt.% ash, 46.29 wt.% volatile matter, and 7.35 wt.% fixed carbon. Elemental analysis of ADR (wt.%, on dry ash-free basis) was 27.33 wt.% C, 3.06 wt.% H, 3.40 wt.% N, 0.14 wt.% S, and 66.06 wt.% O (by difference).

Methods

TG analysis

Prior to bench scale pyrolysis experiments, ADR sample was processed in a thermogravimetric analysis (TGA) to characterize the pyrolysis process in detail. The thermogravimetric experiments were conducted using NETZSCH Simultaneous Thermal Analyzer STA449F3, with a protective gas flow rate of 100 mL/min. Each run utilized a sample mass of 10 mg, and the experiments were performed at heating rates of 10, 20, 30, and 40° C/min from ambient temperature to 900 °C, respectively.

Apparatus and methods

The schematic diagram of the apparatus is shown in Fig. 1. The pyrolysis tests was performed using an innovative infrared heating system and a conventional electric heating system (Hu et al. 2021). Three grams (±0.001 g) of the anaerobic digestion residues was being put into a quartz tube reactor with an inner diameter of 24 mm and a length of 370 mm in each run. With a flow rate of 100 mL/min, 99.999% pure nitrogen served as the carrier gas. The reactor was heated to the pyrolysis temperature (400, 500, 600, and 700 °C) after the air in the reactor had been removed and held for 30 min to guarantee complete conversion of the ADR samples. A quartz collector submerged in − 25 °C ethylene glycol was utilized to condense the pyrolysis vapor. After passing through three acetone washing beakers, the non-condensable gas was measured using a wet gas flowmeter. Pyrolysis experiments were also done under comparable processing conditions utilizing an electrically heated conventional furnace.

Products analysis

By comparing the weights before and after the U-shaped tube, the weight of pyrolysis liquid products was determined. A Karl-Fischer micro-moisture tester was utilized to determine the water content in liquid products (KSL 701, Zibo Kulun). Prior to analysis, the electrolyte was calibrated with filtered water to reach electrolytic equilibrium. We utilized a total of 20 µL of injection and tested the same sample five times. A micro-GC analyzer (INFICON 3000, Switzerland) was used to determine the contents of pyrolysis gas, including H_2, CH_4, CO, CO_2, and C_2-C_3 (C_2H_4, C_2H_6, C_3H_6, and C_3H_8) (Hu et al. 2022). Gas chromatography–mass

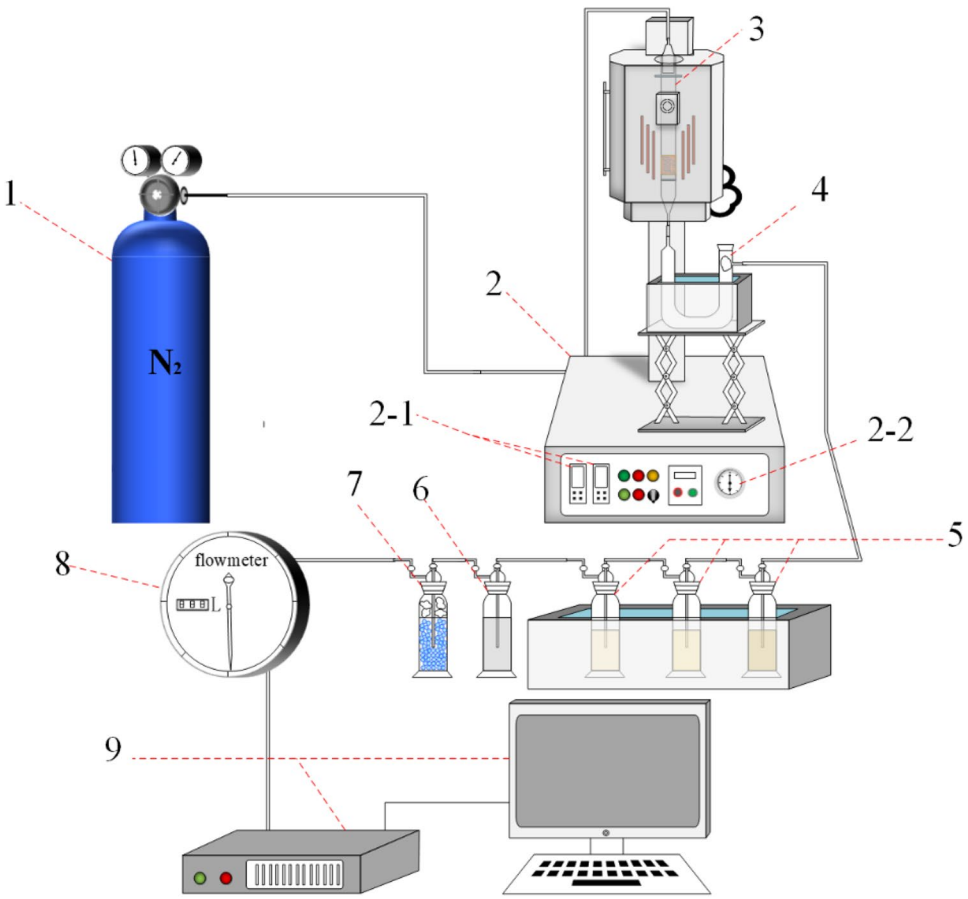

Fig. 1 Schematic diagram of the experimental apparatus. 1 High pressure cylinder, 2 control cabinet, 2–1 temperature controller, 2–2 pressure gage, 3 quartz tube, 4 U-shaped tube, 5 acetone washing bottle, 6 saturated sodium bicarbonate bottle, 7 dry bottle, 8 wet flowmeter, 9 gas chromatograph

spectrometry was used to measure the composition of the bio-oil (GC–MS Shimadzu, GCMS-QP2010 Plus). The temperature of the GC oven was first set at 50 °C for 5 min and further rose at 5 °C/min to 260 °C, finally keeping at this final temperature for 5 min. The carrier gas was high-purity helium at 1 mL/min. The split mode was used, with a 10:1 split ratio. The intake temperature was 250 °C, and the chromatographic column was Rtx-WAX (30 mm*0.25 mm *0.25 m), with 35–500 m/z mass spectrometric collecting range. The spectrum data were compared to the NIST mass spectral library to determine the bio-oil compositions. Fourier transform infrared spectroscopy was adopted to examine the distribution and change of functional groups on the surface of biochar (FTIR). Firstly, the biochar sample and KBr were crushed to a mass ratio of 1:100 (mass ratio) in an agate mortar to prepare transparent wafers. The spectra were analyzed between 400 and 4000 cm^{-1} with a resolution of 4 cm^{-1} and 16 scans. An X-ray diffractometer (XRD, type: D/Max2500pc, Japan) was utilized with filtered Cu-K radiation to identify the phase transformation and crystal structure of biochar. The 2θ scanning ranges of 5 to 55° with a step size of 0.0200° were used to gather data. To investigate the crystalline and amorphous carbon in biochar, Raman measurements were carried out using a Confocal Raman Microspectroscope (LabRAM HR Evolution, France) equipped with a 514.4 nm Ar^{+} laser beam with a spectral resolution of 1 cm^{-1}. A laser with a power of less than 0.4 mW (at the samples) was employed as an excitation source. Raman spectra were recorded in the 500–2000 cm^{-1} range.

Results and discussion

TG analysis

Figure 2 illustrates the TG and DTG curves of the ADR samples. The TG curve indicated that the residual mass of the ADR samples was more than 50%, and this matched well with the high ash content of ADR as determined by elemental analysis. ADR pyrolysis process consisted of three steps: dehydration, pyrolysis, and carbonization. The DTG curves revealed that as the heating rate increased, the maximal weight loss rate of ADR increased as well. The maximum weight loss rate increased from − 2.01 to − 10.35%/min with rising temperature from 10 to 40 °C/min, and its maximum weight loss of the 10 °C/min, 20 °C/min, 30 °C/min, and 40 °C/min were 276 °C, 281 °C, 286 °C, and 290 °C, respectively, which is due to the differences in the heat and mass transfer of sample bed (Mallick et al. 2018; Shahbeig and Nosrati 2020). The first stage occurred mainly between 50 and 150 °C and resulted in the removal of moisture and crustal water from ARD, as well as the breakdown of microorganisms such as bacteria and pathogens. The second weight loss peak of ADR occurred from 160 to 600 °C, with the weight loss from 36.10 to 38.65% at different heating rates. In this stage, two peaks appeared at 290 °C and 320 °C in DTG curves accordingly. Bach and Chen (2017) reported that the decomposition of lipid and protein occurs at 150 ~ 550 °C and 210 ~ 310 °C respectively. ADR is made up of agricultural waste, manure from animals and poultry, and sludge; its weight loss peaks at 290 °C and 320 °C are ascribed in part to protein breakdown. The decomposition of cellulose and hemicellulose lignin occurs mostly at 160 ~ 600 °C (Hu et al. 2016; Sophonrat et al. 2018). Carbonation and decomposition of mineral components such as ash and salts of carboxylic acids may result in the third weight loss peak around 600 ~ 800 °C, indicating a sluggish devolatilized rate (Tsemane et al. 2019). In DTG curves, there was a noticeable thermal lag, and it was hypothesized that thermal hysteresis may negatively affect the products of pyrolysis. Due to the fact that the pyrolysis behavior and product distribution of ADR cannot be investigated using the tiny mg-level sample fed into the TG apparatus, it is critical to perform further study using a bench-scale reactor with g-level.

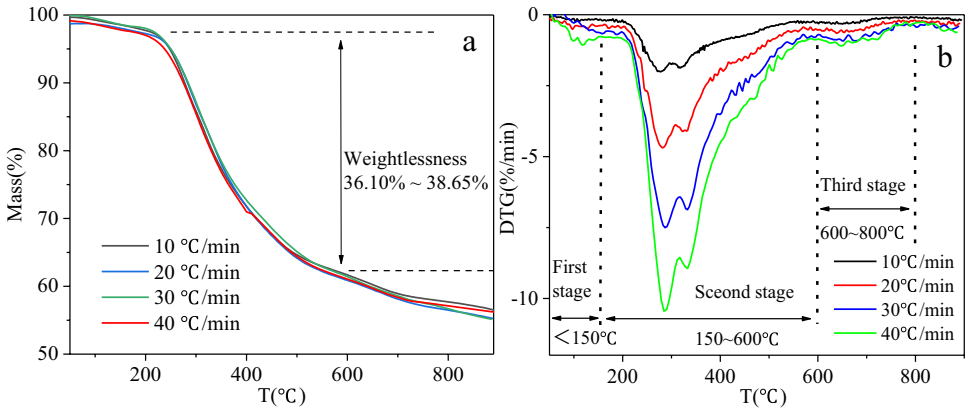

Fig. 2 TG (**a**) and DTG (**b**) curves of ADR

Pyrolysis products distribution

Figure 3 shows the effects of temperature on pyrolysis products distribution using infrared heating (IH) and electric heating (EH) techniques. For both IH and EH, the increase in the temperature increased the bio-oil yield first, reaching to a peak at 500–600 °C, and subsequently reduced yield. In comparison to the results obtained with EH, IH presented a higher overall bio-oil yield but a lower water yield. Notably, the infrared heating (IH) and electric heating (EH) techniques had the largest amount of bio-oil yield at 600 °C and 500 °C, respectively. The bio-oil produced by IH increased from 8.35 to 12.56 wt.% with rising temperature from 400 to 600 °C, but further raising the temperature to 700 °C reduced the bio-oil yield to 11.22 wt.%. The bio-oil produced by EH rose from 9.23 wt.% at 400 °C to a maximum value of 12.12 wt.% at 500 °C, before dropping to 7.80 wt.% as the temperature increased to 700 °C. Both infrared heating and electric heating increased pyrolysis gas yields but decreased biochar yields. As the temperature increased from 400 to 700 °C, the biochar yield dropped from 75.95 to 60.59 wt.% and 69.88 to 59.26 wt.% for IH and EH, respectively. On the other hand, the yield of pyrolysis gas yield rose from 12.46 to 24.57 wt.% and 17.18 to 27.41 wt.%, respectively. The bridge bond began to cleave as the temperature increased during ADR pyrolysis, leading in the generation of free radical groups and large quantities of non-condensable gases. As much heat may be transferred into the inside of ADR particles, accelerating the cleavage of macromolecular organics' alkyl side chains (Gai et al. 2014), which not only generated large condensable gas and small molecule gases but also enhanced the aromatization of biochar. Thermal cleavage of covalent bonds in ADR produced volatiles in a single step that primarily depends on the temperature, while the volatile reactions involve multiple steps and depend on many factors especially the gas phase temperature. Different heating techniques, such as EH and IH, had substantial effects on primary pyrolysis products and volatile repolymerization, resulting in a variation in products distribution (He et al. 2014; Katheklakis et al. 1990).

Figure 4 shows the temperature profiles in reactors. The experimental results indicated that the temperature profile of electrically heated reactor was T1 > T2 > T3, while the infrared heated reactor followed the trend of T1 > T3 > T2. He et al. (2014) discovered that when electric heating was adopted in fixed-bed reactors, a considerable temperature gradient occurred, and consequently the gas phase temperature was much higher than temperature of the materials being processed. When the primary volatiles were exposed to a high-temperature environment, secondary reactions occurred and were exacerbated. This not only deteriorated the quality of oil, but also substantially decreasing the bio-oil production. Infrared heating enabled the material particle to resonate and quickly reach the desired temperature, thus accelerating the heat transfer process. The volatiles produced by IH experienced a lower T2 temperature and a lower rate of secondary reaction of primary volatiles, resulting in an increase in the bio-oil yield (Hu et al. 2017). Due to the temperature differential in EH, the primary volatiles reached a higher T2 temperature and underwent severe secondary reactions, reducing the yield of bio-oil and raising the gas yield (Xu et al. 2019; Zhu et al. 2019).

Bio-oil characterization

Figure 5 illustrates the relative content of main compounds in both IH and EH bio-oil. As can be seen, bio-oil mainly comprised of nitrogen-containing compounds, ketones, alcohols, acids, phenols, alkanes, etc. Infrared heating (IH) presented a greater overall yield of phenolic compounds than EH. Raising temperature increased the phenols contents of bio-oil in IH and EH initially, reaching maximum values of 8.63% and 2.95% at 500 °C and 600 °C, respectively, and subsequently reduced yield. Nitrogen-containing compounds in the IH bio-oil increased with rising temperature, whereas ketones and acids compound reduced. The nitrogen

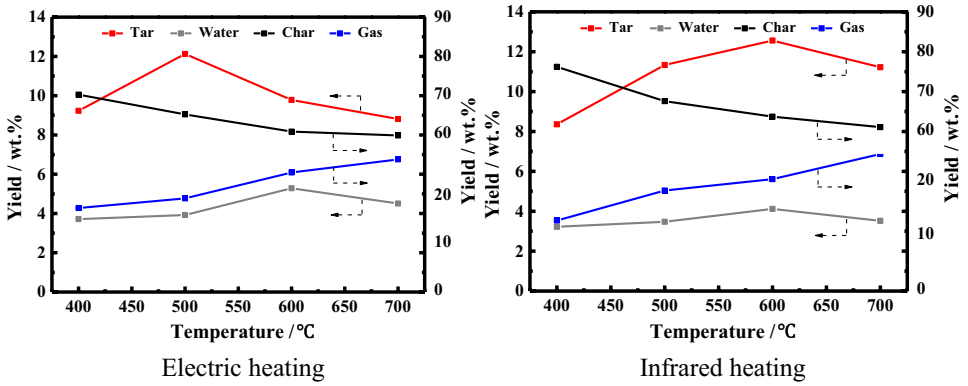

Fig. 3 Effects of temperature on pyrolysis products distribution using infrared heating (IH) and electric heating (EH) techniques

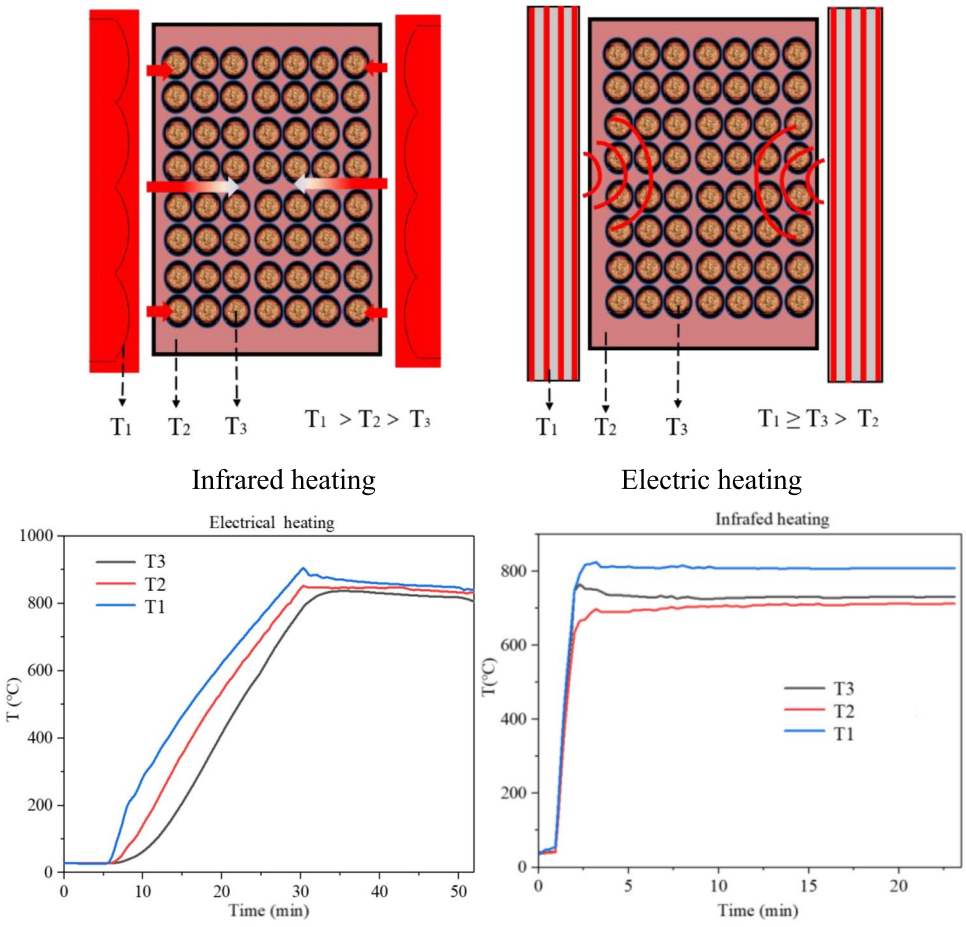

Fig. 4 Profiles of temperature in reactors. T1 refers to the heating temperature; T2 refers to the ambient temperature; T3 refers to the materials temperature

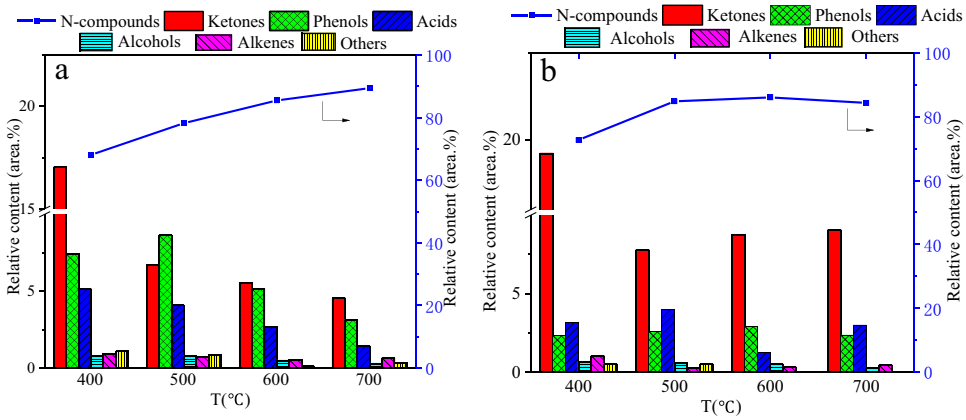

Fig. 5 Relative content of main compounds in both IH and EH bio-oil. **a** IH; **b** EH

compounds yield in IH and EH bio-oils rose 68.14 to 89.43% and 72.69 to 84.29% with rising temperature from 400 to 700 °C, respectively, whereas the contents of ketones and acids of bio-oil in IH decreased from 17.04 to 4.56% and 5.14 to 1.42%, respectively. Nitrogen compounds accounted for a remarkable proportion in total, which may be ascribed to the high nutritional content such as protein, peptides, and nucleic acids in ADR (Parnaudeau and Dignac 2007). As shown in the thermogravimetric study in the "TG analysis" section, a substantial weight loss occurred at 290 °C and 320 °C of the DTG curves, owing to the breakdown of cellulose, hemicellulose, and lignin, as well as nitrogen-containing compounds in the ADR. Ketones, phenolic acids, alcohols, and other oxygen-containing chemicals were discovered in bio-oil, which may be derived from the undigested lignin, cellulose, and hemicellulose in anaerobic

digestion, agreeing well that DTG curve exhibits peaks from 290 to 320 °C. In contrast to the EH, the bio-oil components in the IH changed significantly with increasing temperature. The fast heating by IH increased heat and mass transfer into the particles, allowing the feedstock to reach the desired temperature rapidly, thus intensifying the breakdown of macromolecular organic molecules such as nitrogen and oxygen side chains. EH provided a large temperature gradient between the heat source and the feedstock, which prolonged the reaction time of volatiles, resulting in severe secondary reactions in primary pyrolysis products. Besides, the higher the setting temperature, the larger the temperature gradient in EH reactor, resulting in virtually full volatiles release before the reactor reaches the target temperature. As a consequence of those, the pyrolysis products varied slight with the temperature in EH. The top ten compounds in bio-oil at 500 °C in both reactors are shown in Fig. 6, accounting for about 90% of the total. Piperidine, 1,2-dimethyl-, 4-piperidinone, 2,2,6,6-tetramethyl-, 2-pentanone, and 4-amino-4-methyl- are the top three compounds in bio-oils produced by IH and EH, accounting for more than 50% of the total area. This list is incomplete due to the omission of a few unidentified compounds. The primary difference is that although phenol is the fourth most common compounds in IH bio-oil, it is the ninth most abundant compounds in EH bio-oil, while acetic acid is the fourth most abundant compounds in EH bio-oil. This is because infrared heating promotes pyrolysis of lignin, while EH accelerates cellulose and hemicellulose pyrolysis. In general, the nitrogen-compounds in ADR bio-oil preclude its use as a transportation fuel; it may be used to manufacture plasticizers, rubber softeners, lubricant additives, and insecticide intermediates (Cao et al. 2010), and the extraction of chemical raw materials from ADR bio-oil requires additional research.

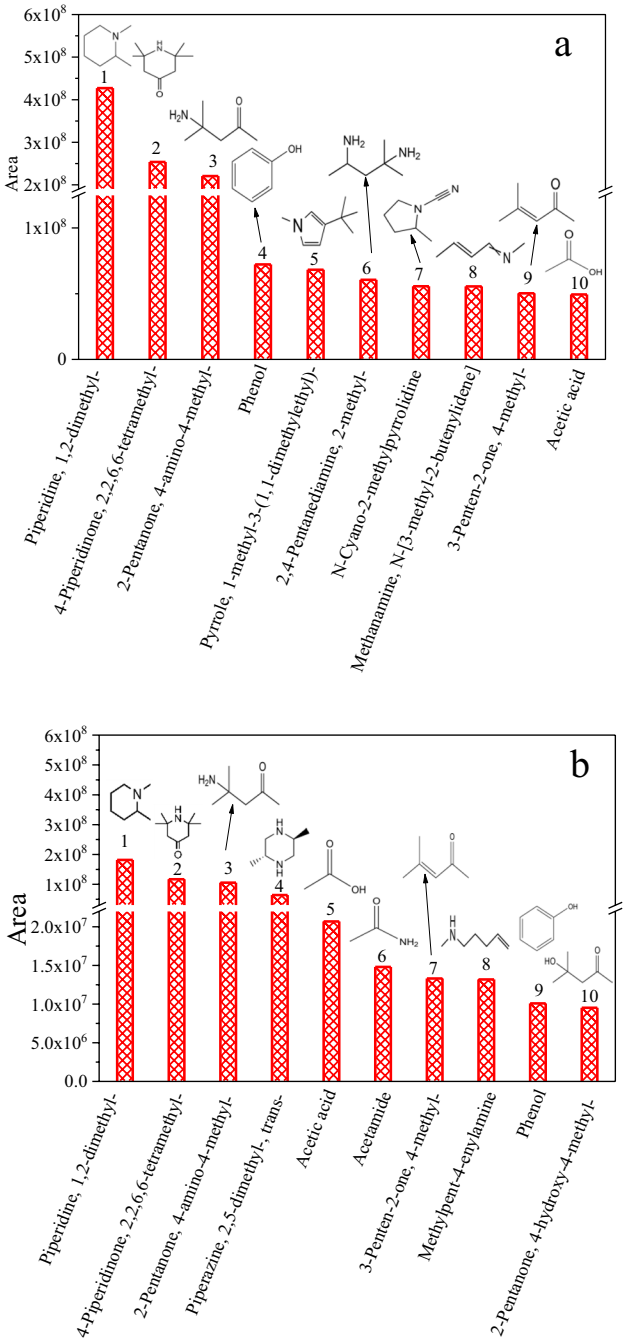

Fig. 6 Top ten compounds in bio-oil **a** IH; **b** EH

Gas composition

Figure 7 illustrates the variation of gas compositions, volumes, and high heating value (HHV). The HHV of gases in both EH and IH increased as the temperature rose; raising temperature from 400 to 700 °C increased the gas HHV in EH and IH from 6.82 MJ/Nm^3 and 8.43 MJ/Nm^3, respectively, to 8.54 MJ/Nm^{3}and 9.67 MJ/Nm^3. Infrared heating has a higher HHV value than electric heating. In most cases, the CO and H_2 contents of IH were much higher than those of EH. As the temperature increased, the CO_2 content of EH and IH decreased. The CO_2 content of EH and IH decreased from 62.14 to 49.91 vol.% and from 55.46 to 41.17 vol.%, respectively, when the temperature was increased from 400 to 700 °C. The decrease in CO and CO_2 contents indicated that side chains of macromolecules in biochar were greatly reduced, which was consistent with the results in the "Biochar characterization" section that the surface structure of biochar became much ordered. The H_2 content in both EH and IH exhibited the opposite trend of CO_2 with temperature variation. IH and EH had the lowest H_2 yields at 500 °C, with 18.11 vol.% and 15.89 vol.%, respectively. When the temperature was increased to 700 °C, the H_2 yields of IH and EH rose to 33.42 vol.% and 26.51 vol.%, respectively. The CH_4 and C_2-C_3 Contents varied slight in both EI and IH.

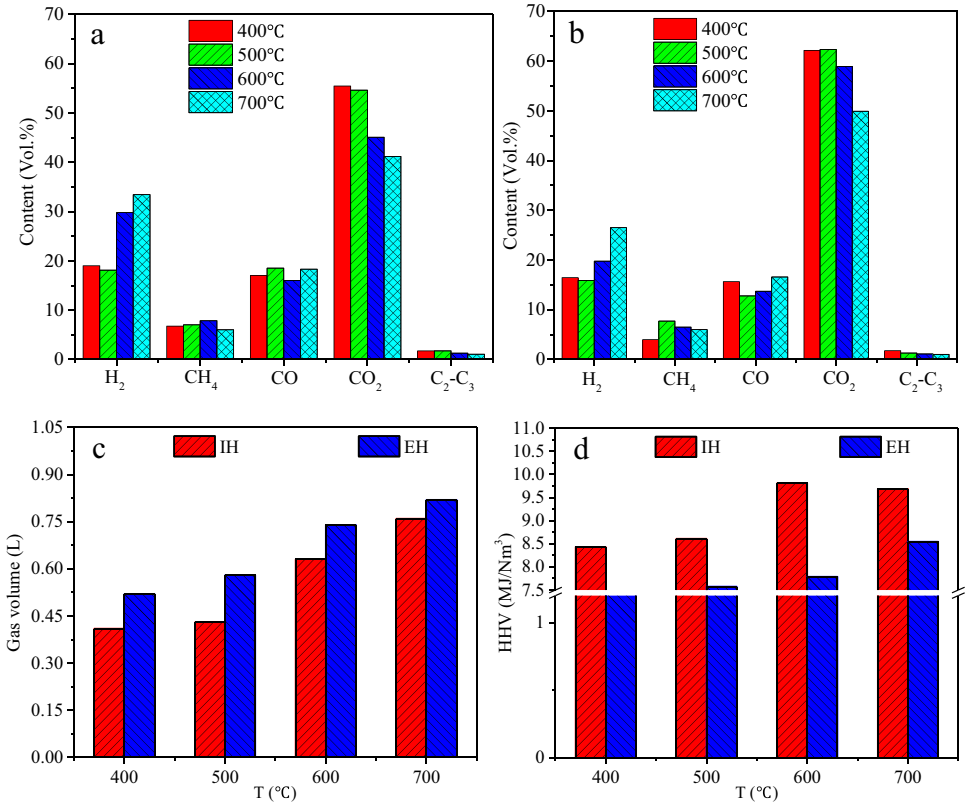

Fig. 7 Composition of gaseous products and its high heating values in the two heating methods; **a** IH; **b** EH; **c** gas volume; **d** gas HHV

Biochar characterization

Raman spectroscopy

Figure 8 shows the Raman spectra of the biochar produced by IH and EH. Raman spectra may be used to determine the locations of the D (defects/disordered) and G (graphite) bands, as well as the intensity ratio of the G and D bands (A_G/A_D) (Asadullah et al. 2010a; Zaida et al. 2007). The Raman signal at 500 ~ 2000 cm^{-1} was mostly attributable to the polyaromatic ring structure of carbon material (Guo et al. 2008). All char samples exhibited two broad bands at about 1350 cm^{-1} and 1580 cm^{-1}. The oxygen-containing structure had a high capacity for Raman scattering, and oxygen-containing structures may increase the Raman intensity through a resonance effect with the linked aromatics (Wu et al. 2014). The D band and G band intensities dropped as the temperature increased, which may be ascribed to the gradual removal of aliphatic and oxygen-containing functional groups during the ADR pyrolysis process, as well as the increased aromatic structure in biochar (Asadullah et al. 2010b).

Figure 9 exhibits the Raman spectra of the IH and EH biochars, as well as its AG/AD values. The G band position of two kinds of biochar shifted slightly to the higher frequencies with rising temperature from 400 to 600 °C but shifted

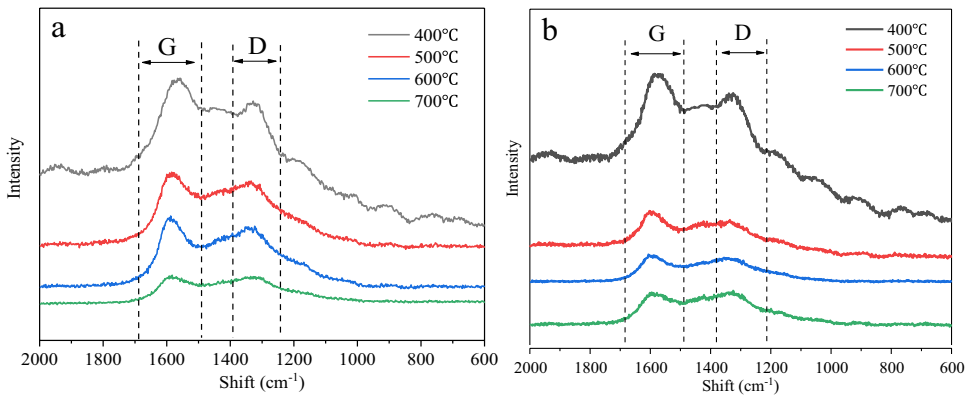

Fig. 8 Raman spectra of the biochar produced by the two heating methods. **a** IH; **b** EH

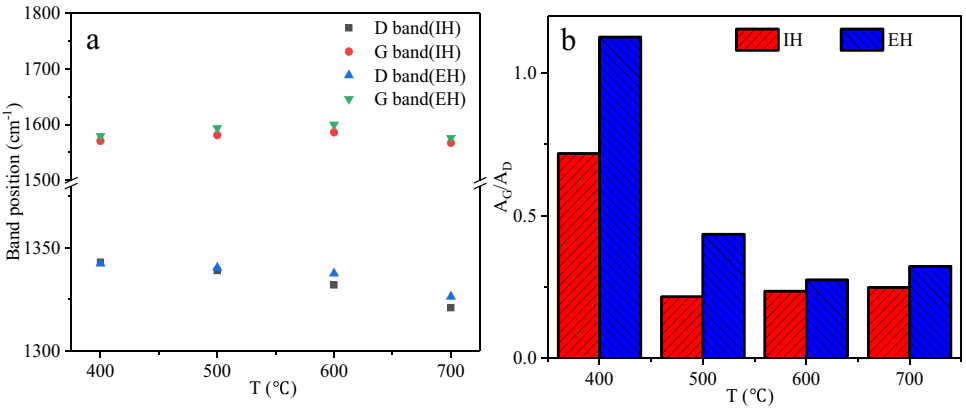

Fig. 9 Band position of G band and D band and ratio of band peak areas A_G/A_D. **a** Band position; **b** ratio of band peak areas A_G/A_D

to the low frequency at 700 °C, owing to the disappearance of tetrahedral bonds and the formation of trigonal bonds in temperature range from 400 to 600 °C. However, when temperature increased, the D band moved to lower frequencies, indicating that as the temperature increased, the disorder of bond angle decreased and the biochar surface structure became much ordered (Jiu et al. 1999; Yamauchi and Kurimoto 2003). The area ratios of G band and D band (A_G/A_D) may be utilized to measure the biochar aromatization. The A_G/A_D at 400 °C is significantly higher than at other temperatures, which may be explained by the fact that biochar heated at 400 °C had much oxygen-containing functional groups, resulting in a stronger Raman spectra (Asadullah et al. 2010b). The ratio of A_G/A_D in IH biochar increased gradually from 0.17 to 0.20 with rising temperature from 500 to 700 °C. This suggests that the increase in the pyrolysis temperature enhanced the degree of aromatization in biochar structure, resulting in a much organized carbon structure. In comparison to IH biochar, the A_G/A_D ratio of EH biochar dropped progressively between 400 and 600 °C but substantially rose at 700 °C, owing to the fact that IH and EH used different heating techniques. Clearly, the A_G/A_D of EH biochar was higher than that of IH at all temperatures, which is due to the slow heating rate and the longer reaction time of ADR in EH. The volatiles were slowly released under the slow heating condition, which is beneficial for maintaining the carbon structure in excellent order. The ADR was quickly heated, and the pyrolysis volatiles released from materials may deteriorate the biochar order. On the other hand, the rapid heating mode of IH significantly reduced the probability of secondary reaction of primary volatiles in this process, whereas the slow heating mode of EH intensified the secondary reaction of the primary volatiles to generate aromatic coke, consequently contributing to a higher A_G/A_D value than 500 °C and 600 °C.

FTIR

Figure 10 illustrates the analysis of FTIR spectra of the biochars produced by EH and IH. The bands intensity in IH biochar was more sensitive with varying temperature than that of EH. With increasing temperature, the amide stretching bands (-CO–NH-) at 1600 ~ 1550 cm^{-1} got weaker until it disappeared entirely at 700 °C. This is due to the complexation of amide functional groups and metals in ADR. Besides, some nitrogen was volatilized and migrated into the liquid phase, where it was incorporated into aromatic compounds through polymerization and aromatization (Xu et al. 2018b).

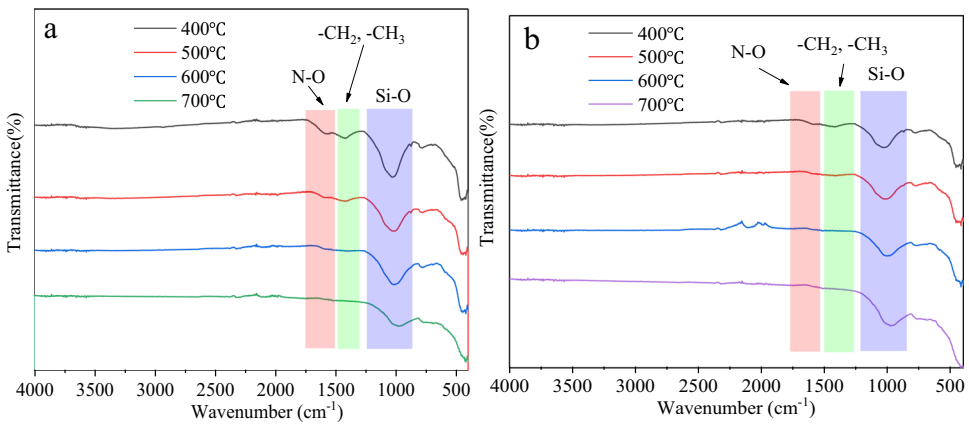

Fig. 10 FTIR spectra of char produced by the two heating methods. **a** IH; **b** EH

The intensity of the bands at approximately 1430 cm^{-1} (for aliphatic chains, including CH_3 and CH_2 groups (Liu et al. 2016)) decreased gradually with rising temperature for all biochar samples, which was attributed to dehydration, demethylation, and elimination of carbonyl and aliphatic groups during aromatic units formation in the chars. In this process, the structure of biochar can become more orderly, which is consistent with Raman spectroscopy results. The intensity between 700 and 900 cm^{-1} was attributed to the emergence of aromatic and heteroaromatic compounds (Lu et al. 2013; Xiao and Yang 2013).These bands showed little change as the temperature increased from 400 to 700 °C, suggesting that the aromatic structure existed prior to the biochar being treated at these temperatures. The aromatic structure of the biochar was critical for carbon sequestration, and if the biochar was strongly aromatic, it had the potential to sequester a large amount of carbon. The bands at about 980 ~ 1028 cm^{-1} correspond to the asymmetric stretching vibration of Si–O-Si in quartz, the stretching vibration of Si–O in aluminosilicates (Zhao et al. 2017), the C-O stretching vibrations of aromatic ring C-O band, and aliphatic C–O–C band, as well as other inorganic substances formed at high temperatures. Both organic and inorganic halogen compounds exhibit stretching vibrations below 600 cm^{-1} (Hossain et al. 2011).

Conclusion

In this work, the effects of temperature on pyrolysis behaviors of anaerobic digestion residues (ADR) were investigated in the fixed-bed reactor with rapid infrared heating and electric heating. The pyrolysis process of ADR consisted mostly of three pyrolysis stages. In both IH and EH, the increase in the temperature increased the bio-oil yield initially, reaching to a peak at 500–600 °C, and thereafter reduced yield. It also elevated the gas yield but decreased the char yield. In contrast to EH, IH presented a higher overall bio-oil yield but a lower water yield. The infrared heating (IH) and electric heating (EH) techniques produced the highest amount of bio-oil yield at 600 °C and 500 °C, respectively, which were 12.56 wt.% and 12.12 wt.%, respectively. IH exhibited a higher CO content and gas HHV but a lower CO_2 content in comparison to the results obtained by EH. The nitrogen compounds in bio-oil accounted for about 80% of the whole ADR bio-oil. Bio-oil in IH had more phenolic compounds than bio-oil in EH, and the phenol content of bio-oil in both IH and EH increased first and then dropped as the pyrolysis temperature rose, reaching the maximum values of 8.63% and 2.95% at 500 °C and 600 °C, respectively. FTIR and Raman results revealed that the structure of ADR biochar becomes more orderly with rising temperature.

Acknowledgements The authors thank Prof. Yang Yang (Bioenergy Research Group, EBRI, Aston University), for his recommendations and revision.

Author contribution Erfeng Hu wrote the original draft and performed the data proofreading. Moshan Li and Chongyang Dai completed the experiments and data analysis. Yishui Tian and Xiaojian Yi helped revise the manuscript and put forward constructive suggestions. Si Shao, Chenhao Li, and Yunfei Zhao participated in the experiment. All authors revised the report and approved the final version before submission.

Funding This study was financially supported by the National Natural Science Foundation of China (52104245), the National Natural Science Foundation of Chongqing (cstc2021jcyj-msxmX0099), the National Modern Agricultural Industrial Technology System (CARS-03–40), and the Fundamental Research Funds of Chongqing City (Nos. CX2019125 and 2019LY41).

Data availability All data generated or analyzed during this study are included in this published article.

Declarations

Ethics approval and consent to participate Not applicable.

Consent for publication Not applicable.

Competing interests The authors declare that they have no competing interests.

References

Ali L, Palamanit A, Techato K, Baloch KA, Jutidamrongphan W (2021) Valorization of rubberwood sawdust and sewage sludge by pyrolysis and co-pyrolysis using agitated bed reactor for producing biofuel or value-added products. Environ Sci Pollut Res 29:1338–1363. https://doi.org/10.1007/s11356-021-15283-6

Asadullah M, Zhang S, Min Z, Yimsiri P, Li CZ (2010a) Effects of biomass char structure on its gasification reactivity. Bioresour Technol 101:7935–7943. https://doi.org/10.1016/j.biortech.2010.05.048

Bach QV, Chen WH (2017) A comprehensive study on pyrolysis kinetics of microalgal biomass. Energy Convers Manage 131:109–116. https://doi.org/10.1016/j.enconman.2016.10.077

Bian B, Lin C, Lv L (2016) Health risk assessment of heavy metals in soil-plant system amended with biogas slurry in Taihu basin, China. Environ Sci Pollut Res 23:16955–16964. https://doi.org/10.1007/s11356-016-6712-3

Cao JP, Zhao XY, Morishita K, Li LY, Xiao XB, Obara R, Wei XY, Takarada T (2010) Triacetonamine formation in a bio-oil from fast pyrolysis of sewage sludge using acetone as the absorption solvent. Bioresour Technol 101:4242–4245. https://doi.org/10.1016/j.biortech.2010.01.031

Du HX, Wu YX, Wu HF, Li FS (2021) Effect of ozone pretreatment on characteristics of dissolved organic matter formed in aerobic and anaerobic digestion of waste-activated sludge. Environ Sci Pollut Res 28:2779–2790. https://doi.org/10.1007/s11356-020-10596-4

Gai RH, Jin LJ, Zhang JB, Wang JY, Hu HQ (2014) Effect of inherent and additional pyrite on the pyrolysis behavior of oil shale. J Anal Appl Pyrolysis 105:342–347. https://doi.org/10.1016/j.jaap.2013.11.022

González-Arias J, Gil MV, Fernández RÁ, Martínez EA, Fernández C (2020) Integrating anaerobic digestion and pyrolysis for treating digestates derived from sewage sludge and fat wastes. Environ Sci Pollut Res 27:32603–32614. https://doi.org/10.1007/s11356-020-09461-1

Guo X, Tay HL, Zhang S, Li CZ (2008) Changes in char structure during the gasification of a victorian brown coal in steam and oxygen at 800 °C. Energ Fuel 22:4034–4038. https://doi.org/10.1021/ef800528c

He WJ, Liu ZY, Liu QY, Ci DH, Lievens C, Guo XF (2014) Behaviors of radical fragments in tar generated from pyrolysis of 4 coals. Fuel 134:375–380. https://doi.org/10.1016/j.fuel.2014.05.064

Hossain MK, Strezov V, Chan KY, Ziolkowski A, Nelson PF (2011) Influence of pyrolysis temperature on production and nutrient properties of wastewater sludge biochar. J Environ Manage 92:223–228. https://doi.org/10.1016/j.jenvman.2010.09.008

Hu M, Chen ZH, Wang SK, Guo DB, Ma CF, Zhou Y, Chen J, Laghari M, Fazal S, Xiao B, Zhang BP, Ma S (2016) Thermogravimetric kinetics of lignocellulosic biomass slow pyrolysis using distributed activation energy model, Fraser-Suzuki deconvolution, and iso-conversional method. Energy Convers Manage 118:1–11. https://doi.org/10.1016/j.enconman.2016.03.058

Hu EF, Zeng X, Wang F, Li Y, Yi XJ, Fu XH (2017) Effects of metallic heating plates on coal pyrolysis behavior in a fixed-bed reactor enhanced with internals. Energ Fuel 31:2716–2721. https://doi.org/10.1021/acs.energyfuels.6b02975

Hu EF, Dai CY, Tian YS, Yang Y, Yi XJ, Li MS, Shao S, Zhao YF (2021) Infrared heated pyrolysis of corn stover: determination of kinetic and thermodynamic parameters. J Anal Appl Pyrolysis 158:105273. https://doi.org/10.1016/j.jaap.2021.105273

Hu EF, Tian YS, Yang Y, Dai CY, Li MS, Li CH, Shao S et al (2022) Pyrolysis behaviors of corn stover in new two-stage rotary kiln with baffle. J Anal Appl Pyrolysis 161:105398. https://doi.org/10.1016/j.jaap.2021.105398

Inyang M, Gao B, Pullammanappallil P, Ding WC, Zimmerman AR (2010) Biochar from anaerobically digested sugarcane bagasse. Bioresour Technol 101:8868–8872. https://doi.org/10.1016/j.biortech.2010.06.088

Jiu JT, Wang H, Cao CB, Zhu HS (1999) The effect of annealing temperature on the structure of diamond-like carbon films by electrodeposition technique. J Mater Sci 34:5205–5209. https://doi.org/10.1023/A:1004711913325

Katheklakis IE, Lin LS, Bartle KD, Kandiyoti R (1990) Effect of freeboard residence time on the molecular mass distributions of fluidized bed pyrolysis tars. Fuel 69:172–176. https://doi.org/10.1016/0016-2361(90)90169-Q

KeChrist O, Sampson M, Golden M, Nwabunwanne N (2017) Slurry utilization and impact of mixing ratio in biogas production. Chem Eng Technol 40:1742–1749. https://doi.org/10.1002/ceat.201600619

Li YQ, Zhang RH, He YF, Zhang CY, Liu XY, Chen C, Liu GQ (2014) Anaerobic co-digestion of chicken manure and corn stover in batch and continuously stirred tank reactor (CSTR). Bioresour Technol 156:342–347. https://doi.org/10.1016/j.biortech.2014.01.054

Liang SB, Han YL, Wei LQ, Mcdonald AG (2015) Production and characterization of bio-oil and bio-char from pyrolysis of potato peel wastes. Biomass Convers Bior 5:237–246. https://doi.org/10.1007/s13399-014-0130-x

Liu XQ, Ding HS, Wang YY, Liu WJ, Jiang, (2016) H pyrolytic temperature dependent and ash catalyzed formation of sludge char with ultra-high adsorption to 1-naphthol. Environ Sci Technol 50:2602–2609. https://doi.org/10.1021/acs.est.5b04536

Liu JX, Huang SM, Chen K, Wang T, Mei M, Li JP (2020) Preparation of biochar from food waste digestate: pyrolysis behavior and product properties. Bioresour Technol 302:122841. https://doi.org/10.1016/j.biortech.2020.122841

Lu HL, Zhang WH, Wang SZ, Zhuang LW, Yang YX, Qiu RL (2013) Characterization of sewage sludge-derived biochars from different feedstocks and pyrolysis temperatures. J Anal Appl Pyrolysis 102:137–143. https://doi.org/10.1016/j.jaap.2013.03.004

Mallick D, Poddar MK, Mahanta P, Moholkar VS (2018) Discernment of synergism in pyrolysis of biomass blends using thermogravimetric analysis. Bioresour Technol 261:294–305. https://doi.org/10.1016/j.biortech.2018.04.011

Meng XY, Dai JL, Zhang Y, Wang XF, Zhu WB, Yuan XF, Yuan HL, Cui ZJ (2018) Composted biogas residue and spent mushroom substrate as a growth medium for tomato and pepper seedlings. J Environ Manage 216:62–69. https://doi.org/10.1016/j.jenvman.2017.09.056

Möller K, Müller T (2012) Effects of anaerobic digestion on digestate nutrient availability and crop growth: a review. Eng Life Sci 12:242–257. https://doi.org/10.1002/elsc.201100085

Neumann J, Binder S, Apfelbacher A, Gasson JR, García PR (2015) A Hornung Production and characterization of a new quality pyrolysis oil, char and syngas from digestate – introducing the thermocatalytic reforming process. J Anal Appl Pyrolysis 113:137–142. https://doi.org/10.1016/j.jaap.2014.11.022

Opatokun SA, Strezov V, Kan T (2015) Product based evaluation of pyrolysis of food waste and its digestate. Energy 92:349–354. https://doi.org/10.1016/j.energy.2015.02.098

Parnaudeau V, Dignac MF (2007) The organic matter composition of various wastewater sludges and their neutral detergent fractions as revealed by pyrolysis-GC/MS. J Anal Appl Pyrolysis 78:140–152. https://doi.org/10.1016/j.jaap.2006.06.002

Shahbeig H, Nosrati M (2020) Pyrolysis of municipal sewage sludge for bioenergy production: thermo-kinetic studies, evolved gas analysis, and techno-socio-economic assessment. Renew Sust Energ Rev 119:109567. https://doi.org/10.1016/j.rser.2019.109567

Siramard S, Bunman Y, Lai DG, Xu GW (2017) Pyrolysis of Huadian oil shale in an infrared heating reactor. Energ Fuel 31:6996–7003. https://doi.org/10.1021/acs.energyfuels.7b00964

Sophonrat N, Sandstrom L, Zaini IN, Yang WH (2018) Stepwise pyrolysis of mixed plastics and paper for separation of oxygenated and hydrocarbon condensates. Appl Energ 229:314–325. https://doi.org/10.1016/j.apenergy.2018.08.006

Tsemane MM, Matjie RH, Bunt JR, Neomagus HWJP, Strydom CA, Waanders FB, Alphen CV, Uwaoma R (2019) Mineralogy and petrology of chars produced by South African caking coals and density-separated fractions during pyrolysis and their effects on caking propensity. Energ Fuel 33:7645–7658. https://doi.org/10.1021/acs.energyfuels.9b01275

Wang J, Hao XX, Liu ZL, Guo ZL, Zhu L, Xiong BJ, Jiang DG, Jiang DM, Shen LY, Li MZ, Kang B, Tang GQ, Bai L (2021) Biochar improves heavy metal passivation during wet anaerobic digestion of pig manure. Environ Sci Pollut Res 28:635–644. https://doi.org/10.1007/s11356-020-10474-z

Wu ZQ, Wang SZ, Zhao J, Chen L, Meng HY (2014) Thermal behavior and char structure evolution of bituminous coal blends with edible fungi residue during co-pyrolysis. Energ Fuel 28:1792–1801. https://doi.org/10.1021/ef500261q

Xiao RR, Yang W (2013) Influence of temperature on organic structure of biomass pyrolysis products. Renew Energ 50:136–141. https://doi.org/10.1016/j.renene.2012.06.028

Xu F, Li Y, Ge X, Yang L, Li Y (2018a) Anaerobic digestion of food waste – challenges and opportunities. Bioresour Technol 247:1047–1058. https://doi.org/10.1016/j.biortech.2017.09.020

Xu QX, Tang SQ, Wang JC, Kob JH (2018b) Pyrolysis kinetics of sewage sludge and its biochar characteristics. Process Saf Environ 115:49–56. https://doi.org/10.1016/j.psep.2017.10.014

Xu SP, Zeng X, Han ZN, Cheng JG, Wu RC, Chen ZH, Masěk O, Fan XF, Xu GW (2019) Quick pyrolysis of a massive coal sample via rapid infrared heating. Appl Energ 242:732–740. https://doi.org/10.1016/j.apenergy.2019.03.079

Xu MY, Yang M, Xie D, Ni J, Meng J, Wang QH, Gao M, Wu CF (2021) Research trend analysis of composting based on Web of Science database. Environ Sci Pollut Res 28:59528–59541. https://doi.org/10.1007/s11356-020-09461-1

Yamauchi S, Kurimoto Y (2003) Raman spectroscopic study on pyrolyzed wood and bark of Japanese cedar: temperature dependence of Raman parameters. J Wood Sci 49:235–240. https://doi.org/10.1007/s10086-002-0462-1

Zaida A, Bar-Ziv E, Radovic LR, Lee YJ (2007) Further development of Raman Microprobe spectroscopy for characterization of char reactivity. P Combust Inst 31:1881–1887. https://doi.org/10.1016/j.proci.200

Zhang J, Yang XN, Shi J, Zhao MY, Yin WQ, Wang XZ, Wang SS, Zhang CG (2021) Carbon matrix of biochar from biomass modeling components facilitates electron transfer from zero-valent iron to Cr(VI). Environ Sci Pollut Res 25:1–13. https://doi.org/10.1007/s11356-021-17713-x

Zhao Y, Liu L, Qiu PH, Xie X, Chen XY, Lin D, Sun SZ (2017) Impacts of chemical fractionation on Zhundong coal's chemical structure and pyrolysis reactivity. Fuel Process Technol 155:144–152. https://doi.org/10.1016/j.fuproc.2016.05.011

Zhu JL, Jin LJ, Li JG, Bao ZX, Hu HQ (2019) Fast pyrolysis behaviors of cedar in an infrared-heated fixed-bed reactor. Bioresour Technol 290:121739. https://doi.org/10.1016/j.biortech.2019.121739